SYMMETRIC AND NONSYMMETRIC BUCKLING OF FINITELY DEFORMED ECCENTRICALLY STIFFENED SHELLS OF REVOLUTION

by

David Bushnell

6-67-66-15

August 1966

Lockheed

PALO ALTO RESEARCH LABORATORY

LOCKHEED MISSILES & SPACE COMPANY • A GROUP DIVISION OF LOCKHEED AIRCRAFT CORPORATION
PALO ALTO, CALIFORNIA

Aerospace Sciences Laboratory

Technical Report: Solid Mechanics

SYMMETRIC AND NONSYMMETRIC BUCKLING OF FINITELY DEFORMED ECCENTRICALLY STIFFENED SHELLS OF REVOLUTION

by

David Bushnell

6-67-66-15 August 1966

This work was sponsored by the LMSC Independent Development Program. The computer time associated with this research was sponsored in part by NASA under NAS 1-6073.

Symmetric and Nonsymmetric Buckling of Finitely Deformed Eccentrically Stiffened Shells of Revolution*

by

David Bushnell**
Lockheed Missiles and Space Company, Palo Alto, California

ABSTRACT

The symmetric and nonsymmetric buckling of axisymmetrically loaded shells of revolution is studied. The analysis is valid for monocoque and eccentrically stiffened shells. Finite prebuckling rotations and other nonlinear prebuckling effects are accounted for in the stability analysis, which is formulated as a linear eigenvalue problem and treated by the method of finite differences. Donnell-type equations are used in the study of nonsymmetric bifurcation buckling and appropriately linearized Reissner equations are used in the study of symmetric bifurcation buckling. Nonlinear Reissner equations are used to obtain the prebuckled state of the shell and to cover the case of large deflection axisymmetric collapse. The boundary conditions are expressed in a general form in order to permit treatment of composite shells or ring supports whose elastic properties are accounted for through stiffness coefficients. The analysis is programmed on a digital computer and numerical results are presented for externally pressurized monocoque torus shells, eccentrically stiffened shallow spherical caps, and monocoque complete spherical shells with local imperfections in the form of flat spots. Good agreement is found with previous independent investigations of the torus and with experimental results on internally stiffened spherical caps. Some significant new conclusions reached are: 1) Finite prebuckling rotations and other nonlinear prebuckling effects do not affect the theoretical buckling loads of torus shells; 2) the eccentricity effect must be included in order to

predict accurately the buckling load of meridionally stiffened spherical caps; and 3) externally pressurized, imperfectly manufactured spherical shells will fail through large-deflection axisymmetric collapse rather than through bifurcation buckling.

* The computer time associated with this research was sponsored in part by the LMSC Independent Development Program and in part by the NASA under contract NAS 1-6073.

** Research Specialist, AIAA Member.

Nomenclature

a	meridional radius of curvature of torus, sphere
A_{ij}	coefficients of constitutive equations, see Ref. 1
b	distance from axis of symmetry to meridional center of curvature of torus
b_2	arc length between circumferential ribs
B_{33}, B_{66}	see equations (5a)
BAll, etc.	boundary condition coefficients at A, see eq. 9
BBll, etc.	boundary condition coefficients at B, see eq. 9
C_{33}	shear modulus of shell wall $C_{33} = E/[2(1 + \nu)]$
E	Young's modulus
G	shear modulus of ribs
H	horizontal force/length
J	torsional stiffness constant for ribs
k^*	curvature of deformed shell
K	Gaussian curvature
M	moment resultant
M_T	$(M_{12} + M_{21})/2$
m	number of meridional stiffeners
N	stress resultant
n	number of circumferential waves in buckling pattern
p	normal pressure
p_{cr}	buckling pressure for complete sphere of thickness t or t_s
R	radius of curvature
R_{imp}	radius of curvature of imperfection in spherical shell
r	horizontal radius from axis of symmetry to middle surface

s	arc length
t	shell wall thickness
u	displacement tangential to undeformed meridian
u_H	horizontal displacement
u_v	vertical displacement
v	circumferential displacement
V	vertical force/length
w	normal displacement
α	angle from centerline to edge of spherical dome; also edge angle of imperfection
β	meridional rotation
λ_{nom}	$[12(1 - \nu^2)]^{1/4}(R/t)^{1/2}\alpha$
λ	$\lambda_{nom}(R/R_{imp})^{1/2}$
ϵ	middle surface strain
$\varkappa$	change in radius of curvature
ν	Poisson's ratio
ψ	stress function for n = 0 case. $\psi = rH$
φ	Airy-type stress function
ρ	loading parameter, e.g. p/p_{cr}
ρ_{cr}	critical loading parameter
θ	circumferential coordinate

Subscripts and superscripts

$( )'$	differentiation with respect to arc length s
$\dot{( )}$	differentiation with respect to circumferential coordinate, θ

$( )_s$	shell wall, not including stiffeners
$( )_1$	pertains to meridional direction
$( )_2$	pertains to circumferential direction
$( )_{12}$	shear resultant, twisting moment, twisting change in curvature
$( )_o$	prebuckling quantity

Introduction

While much analytical and experimental work has been done on the stability of monocoque cylindrical and spherical shells and on eccentrically stiffened cylindrical shells, there exist fewer analytical or experimental studies of more general shells of revolution with more general wall construction. In addition practically all of the work done on shell stability presupposes a prebuckled state of the shell based on linear theory.

The stability problem as formulated here has two parts. In the first part the two equations governing the prebuckled state of an arbitrary, axisymmetrically loaded shell of revolution are solved. These are nonlinear, nonhomogeneous, second-order, ordinary differential equations. Their solution and numerical examples are presented in Ref. 1. The second part involves the solution of a linear eigenvalue problem. Displacements and stresses calculated in the first part appear as known variable coefficients in the two homogeneous, linear, partial differential equations governing stability. The lowest eigenvalue of these equations is the buckling load.

Stability Equations: $n \neq 0$

The general equations governing the stability of shells of revolution when $n \neq 0$ can be simplified by making the so-called "shallow" shell assumptions These assumptions are discussed in Ref. 2. They are:

1. the usual assumptions of Love's first approximation,
2. the assumption that the flexural and extensional strains are of comparable magnitude, or

$$t/R << t\varkappa/\varepsilon \ll \text{Min.}(R/t,\ 1/t\varkappa)$$

where $\varkappa$ is the maximum absolute change of curvature and ε is the maximum absolute middle surface strain.

3. the assumption that

$$KL^2 \ll 1$$

where K is the Gaussian curvature and L is the wavelength of deformation.

The first assumption is basic to almost every engineering shell analysis. The second assumption has two important consequences: (1) Two of the three compatibility equations for the deformed middle surface may be approximated by the similar equations for an inextensional deformation of the middle surface, and (2) a moment resultant divided by a radius of curvature of the middle surface, or multiplied by a change in curvature can be neglected compared to the stress resultants. The third assumption permits the approximate solution of the in-plane equilibrium equations by an Airy-type stress function.

The governing equilibrium equations are:

$$\begin{aligned} &(rN_1)' - r'N_2 + \dot{N}_{12} = 0 \\ &\dot{N}_2 + (rN_{12})' + r'N_{12} = 0 \\ &-(rM_1)'' - \ddot{M}_2/r + (r'M_2)' + \dot{M}_T' + rM_T'/r \\ &\qquad = r(N_1k_1^* + N_2k_2^* - N_{10}\kappa_1 - N_{20}\kappa_2) \end{aligned} \tag{1}$$

and the compatibility equations are

$$\begin{aligned} &(r\kappa_2)' - r'\kappa_1 + \dot{\kappa}_{12} = 0 \\ &\dot{\kappa}_1 + (r\kappa_{12})' + r'\kappa_{12} = 0 \\ &-(r\epsilon_2)'' - \ddot{\epsilon}_1/r + (r'\epsilon_1)' + \dot{\epsilon}_{12}' + r'\dot{\epsilon}_{12}/r \\ &\qquad = -r(\kappa_2k_1^* + \kappa_1k_2^* + \beta_0 Kw') \end{aligned} \tag{2}$$

Equations (1) and (2) are almost analogous, with

$$\begin{aligned} \varkappa_2 &\leftrightarrows N_1 & \varkappa_1 &\leftrightarrows N_2 & \varkappa_{12} &\leftrightarrows N_{12} \\ \epsilon_2 &\leftrightarrows M_1 & \epsilon_1 &\leftrightarrows M_2 & \epsilon_{12} &\leftrightarrows M_T \end{aligned} \tag{3}$$

Equations (1a) and(1b) and equations (2a) and (2b) are satisfied approximately by Airy-type stress and curvature functions:

$$\begin{aligned} N_1 &= \ddot{\varphi}/r^2 + \varphi' r'/r \\ N_2 &= \varphi'' \\ N_{12} &= -(\dot{\varphi}/r)' \\ \varkappa_1 &= w'' \\ \varkappa_2 &= \ddot{w}/r^2 + w' r'/r \\ \varkappa_{12} &= -(\dot{w}/r)' \end{aligned} \tag{4}$$

According to Koiter (Ref. 2) w can be considered a "curvature function", analogous to a stress function. There is no need to define it as the normal displacement. However, in the present investigation, where the displacements from the prebuckled equilibrium state are considered to be infinitesimal, w does represent the actual normal displacement within the accuracy of the "shallow" shell equations.

The final governing equations are written in terms of φ and w by inserting equations (4) into (1c) and (2c), with the constitutive equations:

$$\begin{Bmatrix} \epsilon_1 \\ \epsilon_2 \\ \epsilon_{12} \\ M_1 \\ M_2 \\ M_T \end{Bmatrix} = \begin{bmatrix} A_{11} & A_{12} & 0 & A_{13} & A_{14} & 0 \\ A_{21} & A_{22} & 0 & A_{23} & A_{24} & 0 \\ 0 & 0 & B_{33} & 0 & 0 & 0 \\ A_{31} & A_{32} & 0 & A_{33} & A_{34} & 0 \\ A_{41} & A_{42} & 0 & A_{43} & A_{44} & 0 \\ 0 & 0 & 0 & 0 & 0 & B_{66} \end{bmatrix} \begin{Bmatrix} N_1 \\ N_2 \\ N_{12} \\ \varkappa_1 \\ \varkappa_2 \\ \varkappa_{12} \end{Bmatrix} \tag{5}$$

where the A_{ij} are given for eccentrically stiffened shells of revolution in Ref. 1 and

$$B_{33} = 1/(C_{33}t)$$

$$B_{66} = C_{33}\left(t^3/3 + \frac{G_1 J_1 m}{2\pi r\, C_{33}} + \frac{G_2 J_2}{b_2 C_{33}}\right) \tag{5a}$$

The A_{ij} and B_{kk} are similar to the constants originally determined by Baruch (Ref. 3), who assumed that the stiffeners are "smeared out" and that they follow lines of curvature of the shell. The cross-section of the meridional stiffeners is constant, so that their contribution to the stiffness of a shell of revolution varies inversely as the radius r from the axis of revolution. The eccentricity effect is retained by assuming that the strain varies linearly through the actual thickness of the stiffeners and not through a smeared out or "effective" thickness. The sign convention is shown in Fig. 1. A positive change in curvature is such as to reduce the initial curvature. This same convention was used in Ref. 1.

Two ordinary differential equations of fourth order result when

$$\begin{aligned} \varphi &= \varphi_n(s) \sin n\theta \\ w &= w_n(s) \sin n\theta \end{aligned} \tag{6}$$

are inserted into the partial differential equations of compatibility and equilibrium. The final equations have the form:

$$\begin{aligned} &CB(M,1)\varphi^{iv} + CB(M,2)\varphi''' + CB(M,3)\varphi'' + CB(M,4)\varphi' + CB(M,5)\varphi \\ &\quad + CB(M,6)w^{iv} + CB(M,7)w''' + CB(M,8)w'' + CB(M,9)w' + CB(M,10)w = 0 \end{aligned} \tag{7}$$

where

$$\begin{aligned} CB(M,1) &= -\, r\, A_{22} \\ CB(M,2) &= r'(A_{12} - A_{21} - 2A_{22}) - 2rA'_{22} \\ CB(M,3) &= r'^2 A_{11}/r + n^2(A_{12} + A_{21} + B_{33})/r + rK(A_{22} - A_{12} + 2A_{21}) \\ &\quad - 2r'A'_{21} - rA''_{22} - 2r'A'_{22} + r'A'_{12} + f_1 \end{aligned} \tag{8}$$

$$\begin{aligned} CB(M,4) &= -A_{11}(r'^3/r^2 + 2r'K) + A_{21}(r'K - 2n^2r'/r^2) \\ &\quad - B_{33}n^2r'/r^2 + A'_{21}(2rK + n^2/r - r'^2/r) - r'A''_{21} \\ &\quad + A'_{11}r'^2/r + n^2B'_{33}/r + f_2 \end{aligned}$$

$$\begin{aligned} CB(M,5) &= n^2\{A_{11}(2r'^2/r^2 + K - n^2/r^2) + A_{21}(K + 2r'^2/r^2) \\ &\quad + B_{33}(K + r'^2/r^2)\}/r + n^2A''_{21}/r - r'A'_{11}n^2/r^2 \\ &\quad - r'B'_{33}\, n^2/r^2 + f_3 \end{aligned}$$

The coefficients written as equations (8) are the coefficients of the φ-terms of the compatibility equation. The coefficients of the w-terms and of the equilibrium equation can be obtained by analogy. Table 1 gives the changes which must be made in the A_{ij} and definitions of f_1, f_2, and f_3. In the derivation by analogy of the remaining undefined coefficients, the values given in the first column of Table 1 are replaced by the corresponding values of the other three columns.

The designation CB(M,N) for the numerical coefficients is used in the computer program to be explained below. The row number M denotes the m^{th} equation in the set of $2K + 10$ finite-difference equations generated by dividing the meridian into K intervals, satisfying compatibility and equilibrium at the $K + 1$ points in the domain and satisfying 4 boundary or symmetry conditions at each end of the meridian. In the computer program odd equations are compatibility equations and even equations are equilibrium equations.

Boundary Conditions

The boundary conditions for the stability problem are treated in a manner analogous to that explained in Ref. 1. General boundary conditions can be written in the form:

$$\begin{bmatrix} BA11 & BA12 & BA13 & BA14 & BA15 & BA16 & BA17 & BA18 \\ BA21 & BA22 & BA23 & BA24 & BA25 & BA26 & BA27 & BA28 \\ BA31 & BA32 & BA33 & BA34 & BA35 & BA36 & BA37 & BA38 \\ BA41 & BA42 & BA43 & BA44 & BA45 & BA46 & BA47 & BA48 \\ BB11 & BB12 & BB13 & BB14 & BB15 & BB16 & BB17 & BB18 \\ BB21 & BB22 & BB23 & BB24 & BB25 & BB26 & BB27 & BB28 \\ BB31 & BB32 & BB33 & BB34 & BB35 & BB36 & BB37 & BB38 \\ BB41 & BB42 & BB43 & BB44 & BB45 & BB46 & BB47 & BB48 \end{bmatrix} \begin{Bmatrix} rH \\ M_1 \\ u_H \\ \beta \\ v \\ rN_{12} \\ u_V \\ rV \end{Bmatrix} = 0 \quad (9)$$

The first 4 of equations (9) are the boundary conditions at A (See Fig. 1). The last 4 are the boundary conditions at B . The boundary conditions are given in this general form in order to permit treatment of composite shells in which the elastic properties of adjacent structures are accounted for through their stiffness coefficients. In addition the formulation of the stability problem must be compatible with the formulation of the prebuckling nonlinear analysis. Hence the first four quantities in the column vector of equations (9) are the same as those appearing in equations (14) of Ref. 1.

The boundary condition equations have the form shown in equation (7). Tables 2 and 3 give the coefficients B(I,J) for the forces and displacements normal and tangential to the prebuckled middle surface. These must be resolved in the horizontal and vertical directions for use as shown in equations (9). With regard to the A_{ij} and B_{kk}, the changes shown in Table 1 must be made in order to derive by analogy the coefficients of the w-terms (B(I,J), J = 7 through 10). The functions f_4 through f_{10} are tabulated in Table 3.

The expressions for u and v in terms of the stress function φ and the normal displacement w are obtained by first eliminating v and the s-derivatives of u from the strain-displacement relations:

$$\begin{aligned} \epsilon_1 &= u' + w/R_1 + \beta_o w' \\ \epsilon_2 &= ur'/r + v'/r + w/R_2 \\ \epsilon_{12} &= u'/r + r(v/r)' + \beta_o w'/r \end{aligned} \tag{10}$$

The following equation is found:

$$u''/r + u(rK + r'^2/r) = \dot{\epsilon}_{12} - r\epsilon_2' + r'\epsilon_1 + rw'k_2^* - r'w/R_2 - \beta_o w''/r \tag{11}$$

The circumferential displacement v can be found from equation (10b) and equation (11).

Solution of the Equations

The method of finite differences is used to solve the linear differential equations of the form (7). The set of finite difference equations is arranged as described in Ref. 1 (See Fig. 2 of that reference). Hence the matrix of coefficients is strongly banded about the main diagonal. Efficient machine language subroutines have been written at the Lockheed Missiles and Space Company (Ref. 4) to solve large equation systems whose coefficient matrices are banded.

The derivatives of φ and w are simulated by 5-point central difference formulas and the coefficients of $2M + 8$ algebraic equations are stored in a condensed matrix A. The $2M + 8$ equations correspond to the compatibility equation and the equilibrium equation at M points on the meridian, and 8 boundary conditions, four at each end of the shell.

Stability Equations for n = 0

The stability equations for n = 0 can be derived by carefully specializing the equations valid for $n \neq 0$, or by appropriately modifying the nonlinear prebuckling equations of Ref. 1. When one attempts to solve equations of the form (7) by the finite difference method, the case n = 0 gives rise to numerical difficulties associated with ill-conditioned coefficient matrices. Hence, the n = 0 case is approached by modifying the Reissner-type equations (9), (11), and (15) of Ref. 1. The quantities ψ , β , and $D\psi$ are each split into two parts:

$$\psi = \psi_o + \psi_i \qquad \beta = \beta_o + \beta_i \qquad D\psi = D\psi_o + D\psi_i \tag{12}$$

The prebuckling parts ψ_o , β_o , and $D\psi_o$ are finite; the increments ψ_i , β_i , and $D\psi_i$ are infinitesimal. Since

$$D\psi = \psi - rV(r'R_2/r) \tag{13}$$

and rV , being statically determinate, does not change during buckling, it is clear that $D\psi_i = \psi_i$. The following stability equations result when the right-hand sides of equations (12) are inserted into equations (9), (11), and (15) of Ref. 1, and only linear terms in the increments ψ_i and β_i are retained:

Compatibility: M = 2I + 1

$$\begin{aligned} &C(M,1)\psi_i''' + C(M,2)\psi_i' + [C(M,3) + CNONL(M,3)\beta_o' + CNONL(M,7)\beta_o]\,\psi_i \\ &\quad + C(M,4)\beta_i'' + [CNONL(M,1) + CNONL(M,2)\beta_o + CNONL(M,3)D\psi_o + CNONL(M,4)p]\,\beta_i' \\ &\quad + [CNONL(M,2)\beta_o' + CNONL(M,5) + 2CNONL(M,6)\beta_o + CNONL(M,7)D\psi_o + CNONL(M,8)\,rV \\ &\quad + CNONL(M,9)p]\,\beta_i = 0 \end{aligned} \tag{14}$$

Equilibrium: $M = 2I + 2$

$$C(M,1)\psi_i'' + [CNONL(M,1) + CNONL(M,2)\beta_o]\psi_i' + [C(M,3) + CNONL(M,4)\beta_o' + CNONL(M,8)\beta_o]\psi_i + C(M,4)\beta_i'' + [CNONL(M,3) + CNONL(M,4)D\psi_o + CNONL(M,5)p]\beta_i' + [CNONL(M,6) + 2CNONL(M,7)\beta_o + CNONL(M,8)D\psi_o + CNONL(M,9)rV + CNONL(M,10)p]\beta_i = 0 \quad (15)$$

The boundary condition equations, of which there are two for each endpoint of the meridian, have the form:

$$C(M,2)\psi_i' + [C(M,3) + CNONL(M,3)\beta_o]\psi_i + C(M,5)\beta_i' + [CNONL(M,1) + 2CNONL(M,2)\beta_o + CNONL(M,3)D\psi_o + CNONL(M,4)p]\beta_i = 0 \quad (16)$$

Formulas for C(M,N) and CNONL(M,N) are given as equations (10), (12), and (16) in Ref. 1. As in Ref. 1, the stability equations for n = 0 are solved by simulating the derivatives by 3-point finite-difference formulas at each of the M stations on the meridian. The arrangement of these equations in a condensed matrix is as described in Ref. 1 and above.

Finding the Lowest Eigenvalue

The stability equations in finite difference form are a set of linear, homogeneous, algebraic equations. There exist nontrivial solutions of this set for discrete values of a parameter, in this case a load or pressure parameter. The lowest eigenvalue is the buckling load or pressure. Its value can be obtained by various methods. The determinant of the coefficient matrix can be plotted versus the load in order to find the point where its sign first changes. When the eigenvalue problem has the form

$$(A + \lambda B)x = 0 \tag{17}$$

an iteration scheme (Ref. 5) can be employed to calculate both the lowest eigenvalue and eigenvector.

In this general analysis in which nonlinear prebuckling effects are included, the eigenvalue problem does not have the simple form (17). The eigenvalue parameter λ (load or pressure) does not appear linearly, but manifests itself through the prebuckling meridional rotation β_o, stress resultants N_{10} and N_{20}, and changes in curvature CURV1 and CURV2, which appear in the coefficients of the stability equations. These quantities are related in a nonlinear way to the loading. However, there are many practical shell structures which buckle when β_o is so small that linear theory is still accurate. In such cases the stability equations can be approximated by equations of the form (17) and the power method (Ref. 5) can be used to find the lowest eigenvalue and corresponding eigenvector with a fair degree of accuracy.

When the nonlinear terms are important, such as in the case of bifurcation buckling of externally pressurized shallow spherical caps, the power method can be used to advantage in the following way: The determinant D of coefficients of the stability equations is evaluated for increasing values of the loading parameter ρ, where rather large step sizes in ρ are taken. Figure 2 shows a plot of D versus ρ. There is a ρ-interval, ρ_1 to ρ_2, in which D first changes sign. The load for which D = 0 is approximated by linear interpolation from the endpoints ρ_1 and ρ_2 of the interval. The error in the buckling load is now $D\rho = \rho_3 - \rho_{cr}$. If $D\rho/\rho_{cr} \ll 1$, β_o, N_{10} and N_{20} can be expanded in Taylor series about ρ_3:

$$\beta_o = (\beta_o)_3 + z(d\beta_o/d\rho)_3 \qquad N_{10} = (N_{10})_3 + z(dN_{10}/d\rho)_3$$
$$N_{20} = (N_{20})_3 + z(dN_{20}/d\rho)_3 \tag{18}$$

where $z = \rho - \rho_3$. Similar expansions can be made for the prebuckling changes in curvature CURV1 and CURV2 . The derivatives $d\beta_o/d\rho$, $dN_{10}/d\rho$, etc. are calculated from interpolation formulas such as

$$\left(\frac{dN_{10}}{d\rho}\right)_3 = \frac{L_1(N_{10})_2}{L_2*STEP} + \left(\frac{1}{L_1} + \frac{1}{L_2}\right)(N_{10})_3 - \frac{L_2(N_{10})_1}{L_1*STEP} \tag{19}$$

Subscripts 1, 2, and 3 refer to values corresponding to ρ_1 , ρ_2 , and ρ_3 . The quantities L_1 , L_2 , and STEP are shown in Fig. . A value for z is calculated from the linear system

$$(A + zB)x = 0 \tag{20}$$

through use of the power method. Since $D\rho/\rho_{cr} \ll 1$, convergence is indeed rapid. The new value of ρ is $\rho = \rho_3 + z$. If $|z/\rho_3|$ is less than some preassigned number ERR , calculations for the eigenvalue terminate. If not, new derivatives $(d\beta_o/d\rho)_4$, etc. are calculated, and a new correction factor is calculated from equation (20). Iterations proceed until $|z/\rho| < \text{ERR}$.

The Computer Program

Figure 3 is a flow chart of the computer program used for finding the lowest eigenvalue (buckling load). The boundary condition coefficients (eq. 9), indices for shell geometry and type of loading, and the wave number n are read in from data cards. The buckling load ρ is first found as a

function of the wave number n assuming no prebuckling rotations. Prebuckling membrane stresses are calculated from membrane theory and the power method is used to find the lowest eigenvalue. The wave number n is varied until a minimum $\rho(n)$ is found.

A more accurate value of ρ is then calculated for the critical wave number by including nonlinear prebuckling effects and plotting the stability determinant as described in the text associated with equations (18)-(20).

There are cases in which the wave number corresponding to a minimum value of ρ_{cr} calculated from linear theory is not the same as that for a minimum value of ρ_{cr} calculated from nonlinear theory. For these cases an option is provided in the program through which one can bypass the linear branch and calculate $\rho_{cr}(n)$ from the nonlinear theory only.

The linear branch is provided to save computer time. For a great many shell geometries, use of the membrane prebuckling analysis yields good approximations to ρ_{cr} and the corresponding wave number n. Less trial and error is then needed in the more time-consuming nonlinear prebuckling analysis.

Numerical Results

The computer program based on the stability theory described above has been used to calculate prebuckling deformations and buckling loads and modes for several types of shells. The program was checked by performing calculations for externally pressurized shallow monocoque spherical caps. The results agreed with the findings of Huang (Ref. 6). The program was further evaluated by calculating buckling loads for monocoque cylinders and conical frustums under hydrostatic compression. Results agreed with the loads calculated in Ref. 7 and Ref. 8, respectively. Calculations were also made

for an axially compressed cylindrical shell reinforced by external stringers of rectangular cross-section. The buckling load agreed with that found in Ref. 9.

Buckling of a Torus under Hydrostatic Compression

In all of the numerical examples listed above, the "shallow" shell theory is clearly accurate, since the shell is either geometrically shallow, or it buckles into a fairly large number of waves. In order to further evaluate the accuracy of the theory, the more marginal case of the monocoque torus was studied. Sobel (Ref. 10) has recently obtained buckling loads for a wide range of torus geometries. His calculations for $n \neq 0$ are based on more accurate shell stability equations, wherein the second and third assumptions (see page 1) of this analysis are not made. However, Sobel does not include prebuckling rotations and nonlinear prebuckling effects in his work.

Numerical results from the asymptotic analysis of Jordan (Ref. 11) for $n = 0$ as well as Sobel's results for $n = 0$ are directly comparable to the results of this analysis, since the shallow shell assumptions are not made in this case. Both Jordan's analysis and the analysis of this paper when $n = 0$ are based on Reissner's equations (Ref. 12).

Table 4 lists the buckling loads from the three independent investigations for $a/t = 100$ and various values of b/a and n. The loads in the column labeled "this analysis" were calculated both from the linear theory and from the more exact theory in which prebuckling rotations and nonlinear prebuckling effects are included in the stability equations. Both theories yielded the same buckling loads for all values of b/a and n.

When $b/a < 7$ and $n \neq 1$ the three analyses agree. The large discrepancy in the buckling loads for $n = 1$ could be due to the shallow shell approximation, although this is not certain. The agreement deteriorates for increasing

b/a. When b/a is large the major terms in the governing equations tend to cancel, leaving small terms to determine the behavior of the torus. These small terms differ in the shallow shell and non-shallow shell analyses.

When n = 0 and b/a is large, the lack of agreement between the present results and Sobel's results is probably due to the assumption in this paper that the vertical force/length V is statically determinate and hence does not change during buckling. However, V is not statically determinate for the torus, since the meridian is doubly-connected. When b/a is small the deformations are concentrated near the crown, and V at the equator can be very accurately calculated from membrane theory. For large b/a this is no longer true, since the buckling deformations are almost inextensional.

Eccentrically Stiffened Shallow Spherical Dome

It is possible with the theory described above to calculate buckling loads for eccentrically stiffened shallow spherical domes of the same geometry as some of those tested by Meyer and Bellifante (Ref. 13). It should be emphasized that this analysis applies only to the general instability mode of failure. In Ref. 13 the domes are referred to as M-2, M-3, and M-4. They are stiffened meridionally by internal ribs of rectangular cross-section. The material of the test domes was Bakelite with a modulus E = 465,000 psi and a Poisson's ratio ν =0.37. The geometry of the domes is given in Table 5, and the buckling loads in Table 6. All of the shells were clamped at the edge.

Photographs in Ref. 13 of buckled shell models M-2, M-3, and M-4 indicate that the mode of failure was general instability. Buckling patterns with 8 circumferential waves formed in all three cases.

The results summarized in Table 6 (ρ_1) indicate that theoretically model M-2 should buckle into 9 waves, M-3 into 8 waves, and M-4 into 11 waves. However, the buckling load ρ_1 is not strongly dependent on the wave number, and it is likely that during the large postbuckling displacements the wave number changes in order to maintain some kind of "least energy" symmetry with respect to the stringers. No such preferred circumferential orientation is possible in this theory, since the stiffeners are "smeared out."

Two interesting phenomena are evident from Table 6. Of great importance to the designer is the fact that external stiffening raises the buckling load (ρ_2) for the same structural weight. A similar phenomenon has been noted by several investigators in the theory of axially compressed, eccentrically stiffened cylindrical shells.

Another interesting point is that the theory based on the membrane prebuckling analysis with $\beta_o = 0$ yields lower buckling loads (ρ_3) for M-3 and M-4 than does the more exact analysis including prebuckling meridional rotations and nonlinear prebuckling effects. This behavior is the reverse of that for shallow monocoque domes. In Ref. 6 Huang shows that the buckling load of a shallow clamped cap, calculated by assuming uniform prebuckling displacement and stress, is always greater than the buckling load of a complete sphere (see Fig. 6, Ref. 6). The load calculated from the "exact" analysis is always less than the buckling load of a complete sphere (see Fig. 7, Ref. 6).

Figure 4 shows the prebuckling deflection at ρ_{cr} and the buckling mode shape for n = 11, model M-4. The shapes are similar to those for an externally pressurized monocoque spherical cap, clamped at the edge.

Imperfect Spherical Shells

In Ref. 1 the external pressures at which imperfect spherical shells collapse axisymmetrically are calculated. The local geometry of the shells is as shown in Fig. 5. No attempt is made in Ref. 1 to calculate the loads, if such exist, at which the deformed symmetric prebuckled equilibrium state becomes unstable and bifurcation to a nonsymmetric equilibrium state occurs.

In the present analysis, it has been found that for $0 < R_{imp}/R \leq 1.4$, axisymmetric collapse occurs before bifurcation buckling when λ is less than about 5.7, and bifurcation buckling occurs first when λ is greater than about 5.7. The same rule of thumb applies to shallow spherical caps clamped at their edges.

Figure 5 shows the prebuckling deflection and buckling mode shape for an imperfect spherical shell with $\lambda_{nom} = 7$, $R_{imp}/R = 1.4$, and $R/t = 100$. The boundary conditions for the prebuckling equations are $\beta = M_1 = 0$ as s becomes large. The boundary conditions for the stability equations are $\beta = M_1 = v = u_v = 0$ as s becomes large. These conditions are applied at a distance $3.3(Rt)^{1/2}$ from the edge of the imperfection. They assure that the uniform membrane state is approached as s becomes large, and hence they simulate the remainder of the spherical shell. From Fig. 5 it is seen that practically all of the buckling deformation takes place in the imperfect portion of the shell. Therefore, it is reasonable to expect that the bifurcation behavior of an imperfect spherical shell will resemble that of a spherical cap with the same geometry as the imperfection and clamped at α.

Figure 6 shows the stability curves for three imperfect spherical shells with R_{imp}/R = 1.05, 1.15, and 1.40. The dotted curve represents the geometric parameter λ for the imperfect portion. It is seen that indeed the imperfect portion does behave almost as though it were a cap clamped at its edge.

In actual practice, it is unlikely that imperfections with $\lambda_{nom} > 6$ will occur while a spherical shell is being manufactured or in service. Tolerances on spherical shells are usually expressed in terms of deviations from sphericity. As can be seen from Fig. 12 of Ref. 1, the critical collapse loads for given deviations from sphericity occur when $\lambda_{nom} < 5$ for any value of R_{imp}/R .

REFERENCES

1. Bushnell, D., "Nonlinear analysis of shells of revolution," Presented at the 4th Aerospace Sciences Meeting, Los Angeles, June 27-29, 1966 (AIAA Paper No. 66-529)
2. Koiter, W. T., "On the nonlinear theory of thin elastic shells," Report 310, Dept. of Mechanical Engineering, Technological Univ., Delft
3. Baruch, M., "Equilibrium and stability equations for stiffened shells," The Sixth Annual Conference on Aviation and Astronautaics, Feb. 24-25, 1964, Tel Aviv and Haifa
4. Tsui, E. Y. W., Brogan, F. A., and Stern, P., "Juncture stress fields in multicellular structures," Vol. 1, LMSC Rept. M-77-65-5, Aug 1965
5. Bodewig, F., Matrix Calculus, North-Holland Publishing Co., Amsterdam, 1959
6. Huang, N-C, "Unsymmetrical buckling of thin shallow spherical shells," J. App. Mech., 31, 447-457, (1964)
7. Sobel, L. H., "Effect of boundary conditions on the stability of cylinders subject to lateral and axial pressures," AIAA J., 2, 1437-1440, (1964)
8. Famili, J., "Asymmetric buckling of finitely deformed conical shells," AIAA J., 3, 1456-1461, (1965)
9. Stuhlman, C., DeLuzio, A., and Almroth, B., "Influence of stiffener eccentricity and end moment on stability of cylinders in compression," AIAA J., 4, 872-877, (1966)
10. Sobel, L. H. and Flügge, W., "Stability of toroidal shells under uniform external pressure," LMSC Rept. 6-75-65-40, Sept 1966
11. Jordan, P. F., "Vibration and buckling of pressurized torus shells," presented at the 4th Aerospace Sciences meeting, Los Angeles, June 27-29, 1966 (AIAA Paper No. 66-445

12. Reissner, E., "On axisymmetrical deformations of thin shells of revolution," Proc. of Symposia in Applied Mathematics, Vol. III, (McGraw-Hill, 1950) p. 45-46

13. Meyer, R. R. and Bellifante, R. J., "Fabrication and experimental evaluation of common domes having waffle-like stiffening," Douglas Rept. SM-47742, Nov 1964

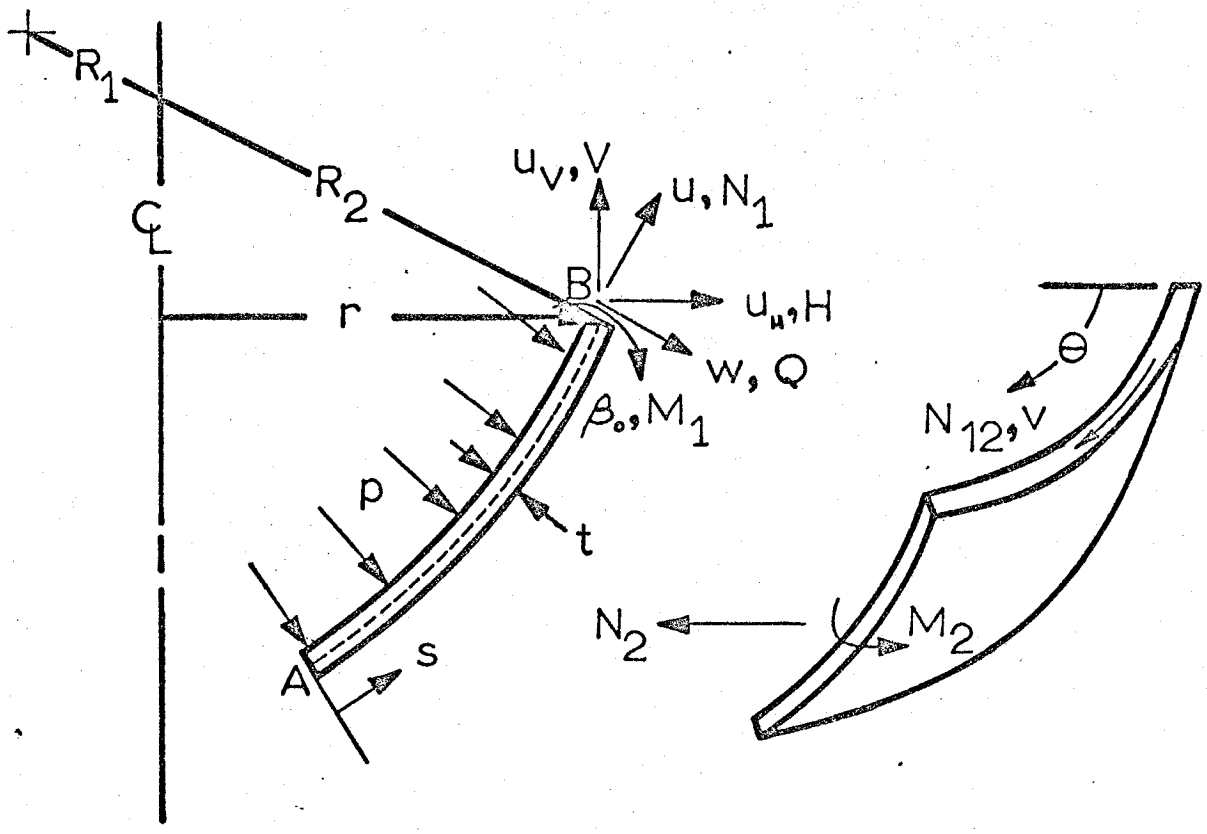

FIG. 1 - COORDINATES, GEOMETRY, LOADS, DISPLACEMENTS & STRESSES

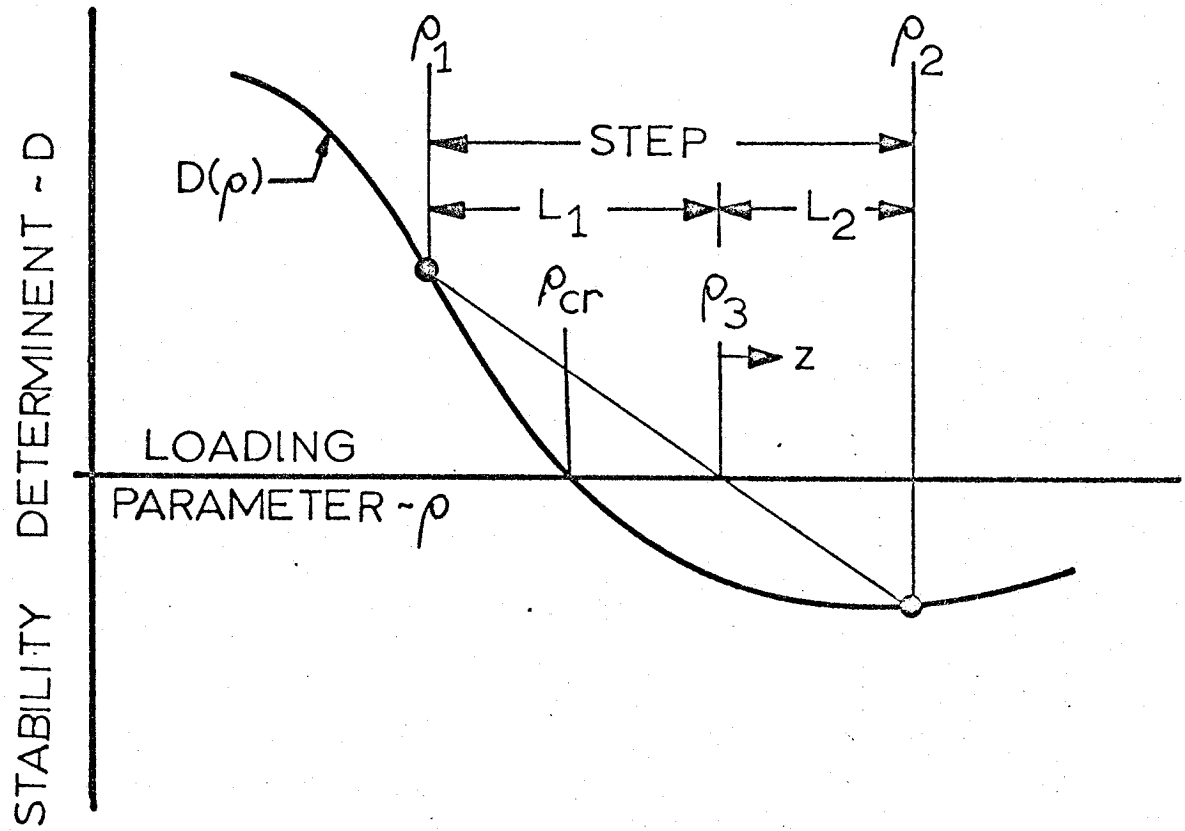

FIG. 2 - DETERMINANT PLOT

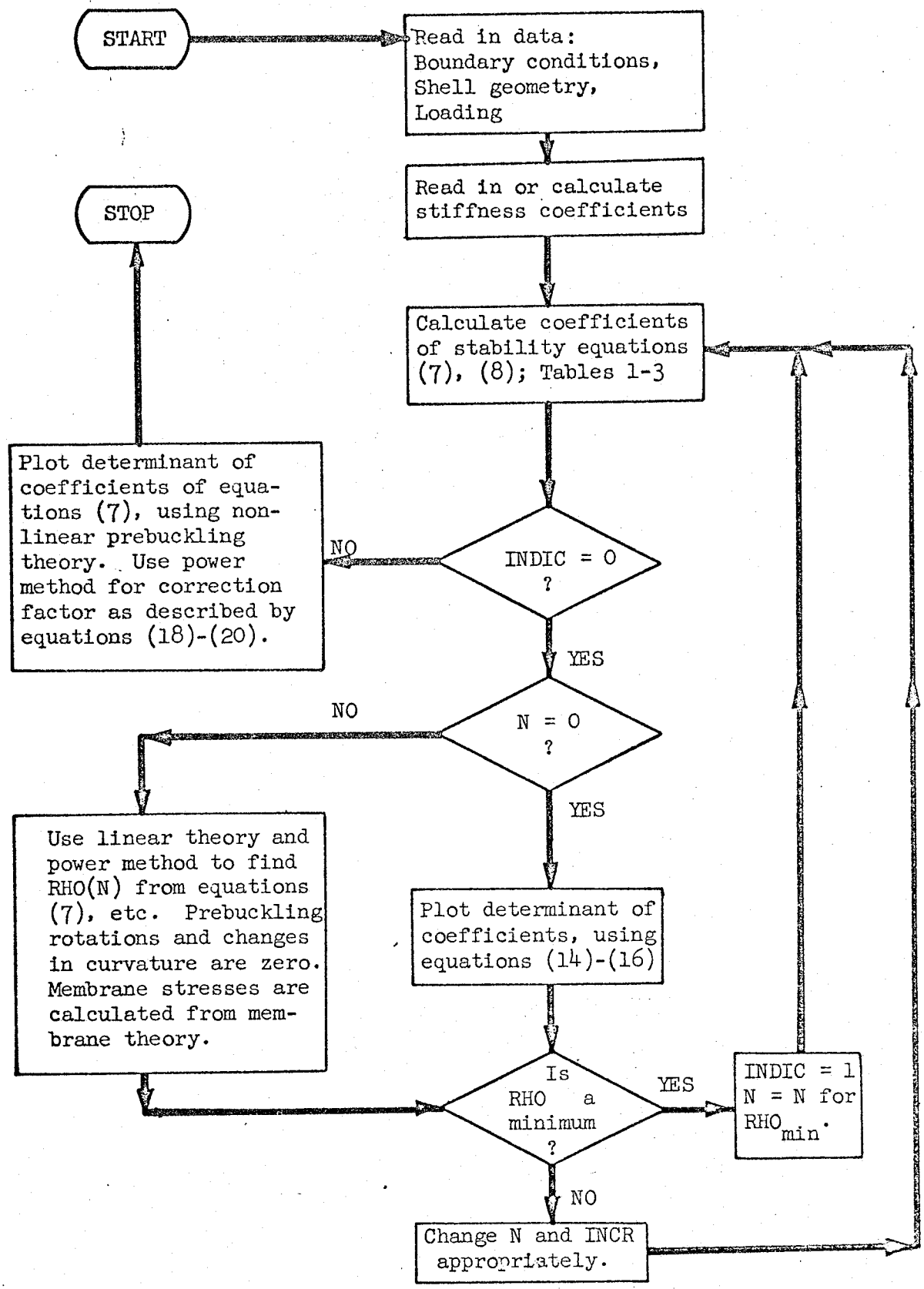

Figure 3 Flow Chart for Computer Program

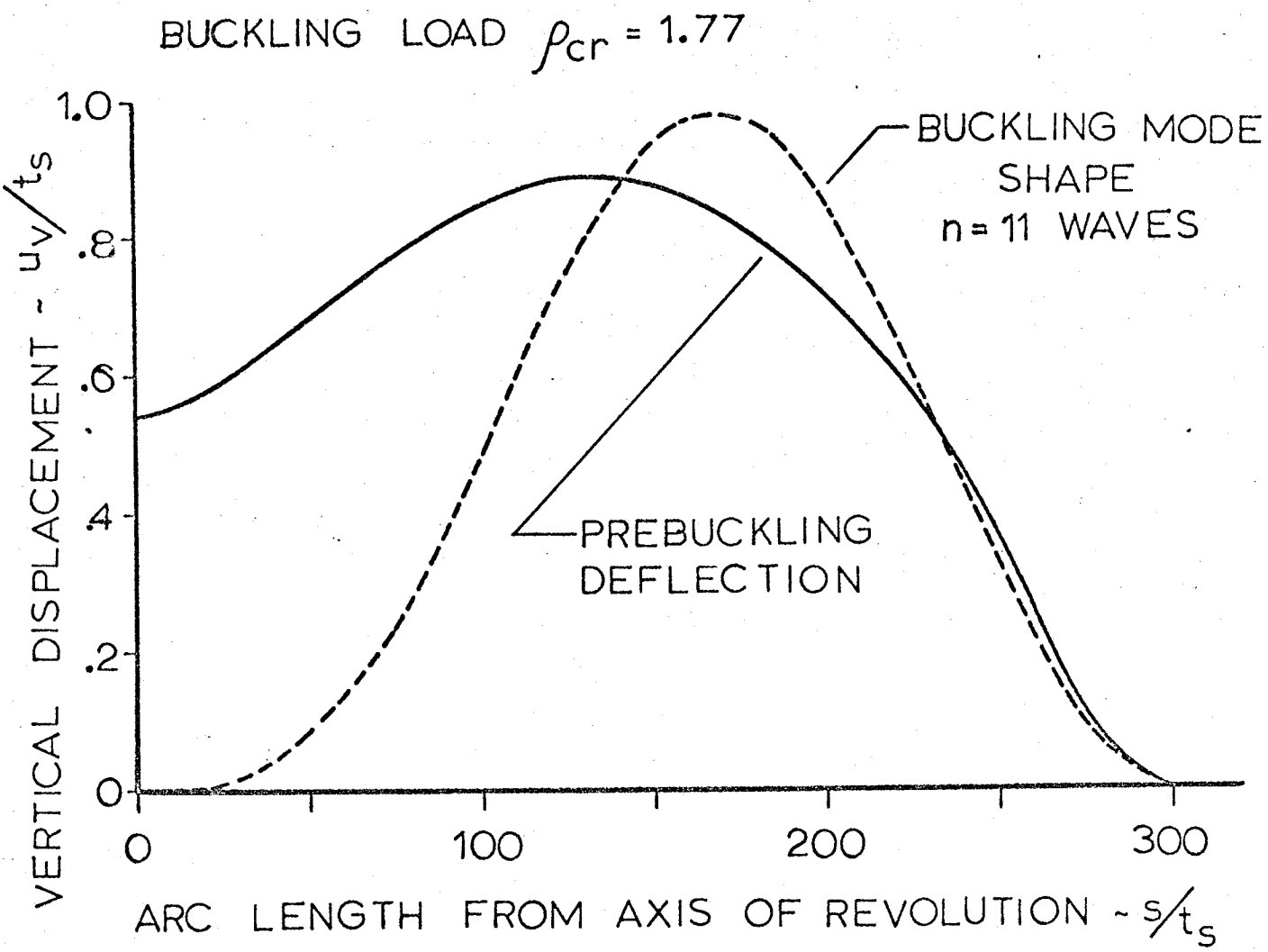

Fig. 4 Prebuckling Deflection and Buckling Mode Shape for Meridionally Stiffened Spherical Cap - Model M-4 of Ref. 13

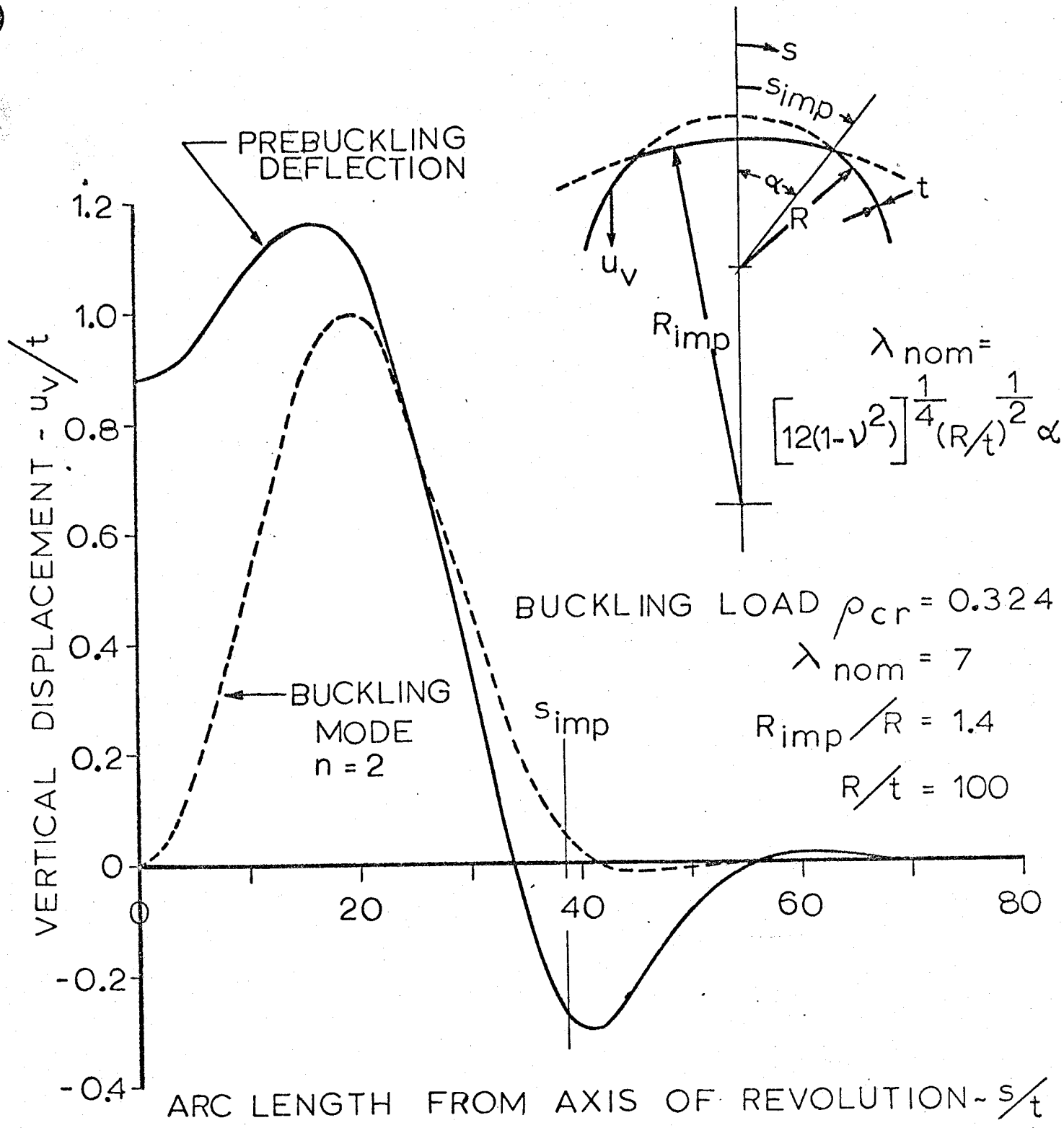

Fig. 5 Prebuckling Deflection and Buckling Mode for Imperfect Spherical Shell

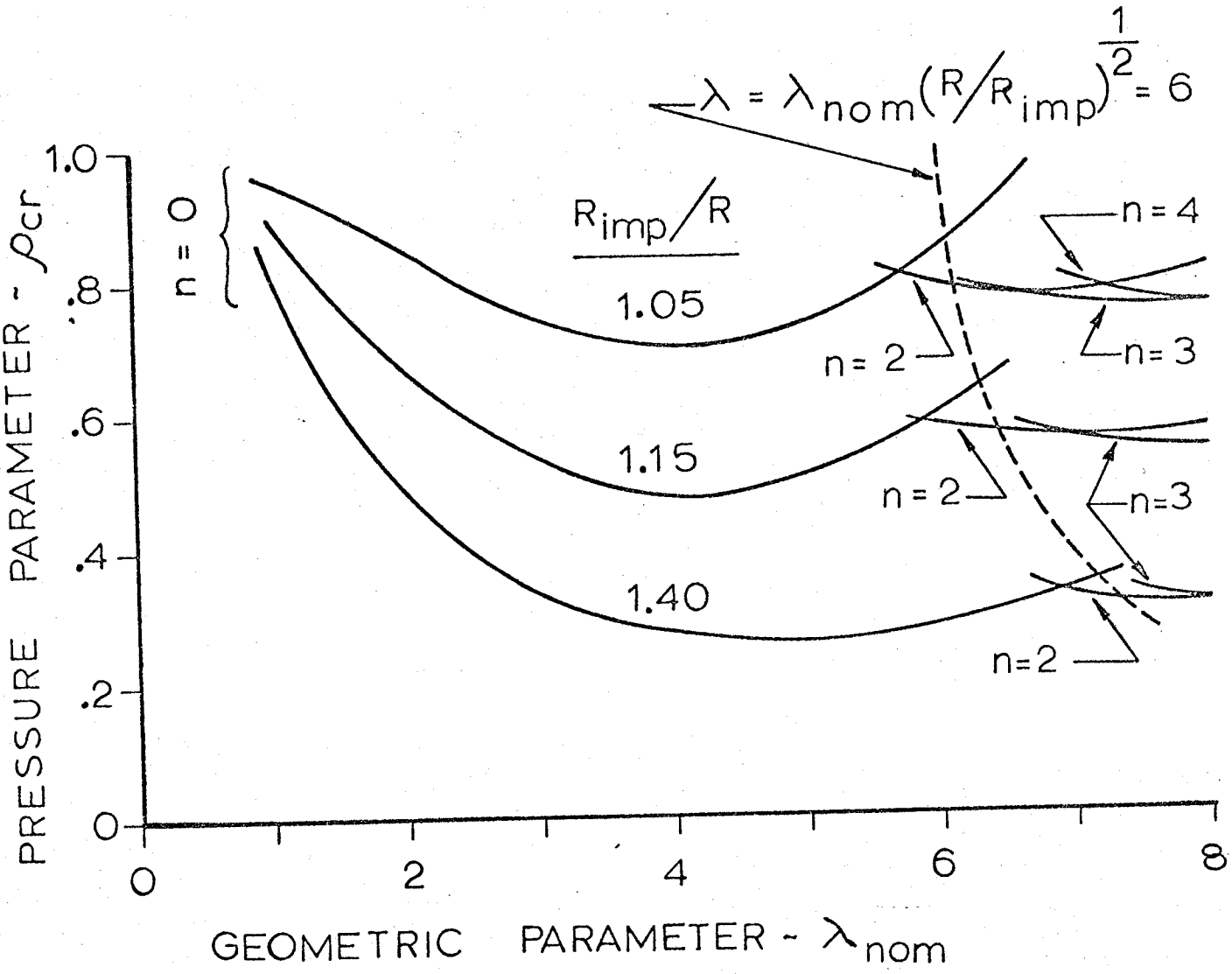

Fig. 6 Stability Loci for Imperfect Spherical Shells, Including Bifurcation Buckling

Table 1

Changes in A_{ij} and Definitions of f_k for the Coefficients CB(M,N) of the Compatibility and Equilibrium Equations

Compatibility		Equilibrium	
φ-terms CB(M,N), N = 1 to 5 replace	w-terms CB(M,N), N = 6 to 10 by	φ-terms CB(M,N), N = 1 to 5 by	w-terms CB(M,N), N = 6 to 10 by
N	N + 5	N	N + 5
A_{11}	A_{14}	A_{41}	A_{44}
A_{12}	A_{13}	A_{42}	A_{43}
A_{21}	A_{24}	A_{31}	A_{34}
A_{22}	A_{23}	A_{32}	A_{33}
B_{33}	0	0	B_{66}
$f_1 = 0$	$f_1 = rk_2^*$	$f_1 = -rk_2^*$	$f_1 = rN_{10}$
$f_2 = 0$	$f_2 = r'k_1^* + \beta_o rK$	$f_2 = - r'k_1^*$	$f_2 = r'N_{20}$
$f_3 = 0$	$f_3 = -n^2k_1^*/r$	$f_3 = n^2k_1^*/r$	$f_3 = -n^2N_{20}/r$

Table 2

Coefficients for Tangential and Normal Forces and Displacements $n \neq 0$

	φ''' B(I,2)	φ'' B(I,3)	φ' B(I,4)	φ B(I,5)
rN_1			r'	$-n^2/r$
rQ	$-rA_{32}$	$r'(A_{42} - A_{31} - A_{32}) - rA'_{32}$	$r'^2A_{41}/r - r'A'_{31} + A_{31}(rK+n^2/r) + f_4$	$-r'n^2(A_{41}+A_{31})/r^2 + n^2A'_{31}/r + f_5$
rN_{12}			$- n$	nr'/r
M_1		A_{32}	$A_{31}r'/r$	$-A_{31}n^2/r^2$
u	$\frac{-rA_{22}}{FACT^*}$	$\frac{-rA'_{22}}{FACT}$	$\{A_{11}r'^2/r + B_{33}n^2/r + A_{21}(r^2K+n^2+r'^2)/r - r'A'_{21} + f_6\}/FACT$	$\{-r'n^2(A_{11}+2A_{21}+B_{33})/r^2 + n^2A'_{21}/r + f_7\}/FACT$
w				f_8
v	$r'u/n$	$(r'u - rA_{22})/n$	$(r'u - r'A_{21})/n$	$(r'u + A_{21}n^2/r)/n + f_9$
β			f_{10}	

*FACT = $rK + r'^2/r - n^2/r$

Table 3

Definitions of f_k for the Boundary Conditions

φ-terms, B(I,J), J = 2 to 5	w-terms, B(I,J), J = 7 to 10
$f_4 = \beta_o r'$	$f_4 = rN_{10}$
$f_5 = - n^2\beta_o/r$	$f_5 = - n^2 r' B_{66}/r^2$
$f_6 = 0$	$f_6 = rk_2^*$
$f_7 = 0$	$f_7 = - r'/R_2 + n^2\beta_o/r$
$f_8 = 0$	$f_8 = 1.0$
$f_9 = 0$	$f_9 = r/(nR_2)$
$f_{10} = 0$	$f_{10} = 1.0$

Table 4

Torus Buckling Loads for a/t = 100

b/a	n	$(p/E) \times 10^6$		
		This Analysis	Sobel	Jordan
1.2	0	3.52	3.73	3.54
	1	3.60		
	2	5.05	5.20	
2.0	0	2.54	2.68	2.52
	1	2.48	10.99	
	2	2.83	2.81	
	3	3.26	3.40	
2.8	0	1.99	2.15	2.01
	1	1.98		
	2	2.22	2.21	
4.0	0	1.61	1.73	1.58
	1	1.56	6.83	
	2	1.72	1.75	
	3	1.87	1.92	
7.0	0	1.10	1.24	1.09
	1	1.07		
	2	1.13	1.23	
30.0	0	0.444	0.547	0.414
	2	0.406	0.529	
100.0	0	0.172	0.387	0.185
	2	0.149	0.370	

Table 5

Geometry for Meridionally Stiffened Domes

Dome Designation from Ref. 13	Number of Stiffeners	Shell and Stiffener Geometry in Inches					
		a	t_s	b	c	d	α
M-2	26	20	.0349	0	.0191	.30	.41
M-3	26	20	.0349	.25	.0191	.30	.41
M-4	38	20	.0272	0	.0239	.30	.41

Table 6

Buckling Loads for Meridionally Stiffened Spherical Domes

Dome Designation	Wave Number n	Buckling Loads $\rho = p/p_{cr}$* Experimental ρ_{exp}	Nonlinear Theory Internal Stiffening ρ_1	Nonlinear Theory External Stiffening ρ_2	Linear Theory Internal Stiffening ρ_3
M-2	7	1.19	1.31	1.46	1.38
	8		1.26		1.31
	9		1.24		1.28
	10		1.25		1.27
M-3	7	1.63		2.28	1.67
	8		1.70		1.58
	9		1.68		1.54
	10		1.70		1.53
M-4	7	1.59	1.86	2.21	1.70
	8		1.63		1.57
	9		1.57		1.50
	10		1.54		1.45
	11		1.54		1.44
	12		1.56		1.44

*$p_{cr} = 2E(t_s/a)^2/[3(1 - \nu^2)]^{1/2}$